Effects of interface bonding configuration on photoluminescence of ZnO quantum dots–SiO_xN_y nanocomposite films

Yu-Yun Peng and Tsung-Eong Hsieh[a)]
Department of Materials Science and Engineering, National Chiao Tung University, Hsinchu, Taiwan 300, Republic of China

Chia-Hung Hsu
Research Division, National Synchrotron Radiation Research Center (NSRRC), Hsinchu, Taiwan 300, Republic of China

(Received 3 September 2007; accepted 15 January 2008)

Nanocomposite films containing ZnO quantum dots (QDs) and SiO_xN_y matrix were prepared by target-attached radio frequency sputtering. Photoluminescence (PL) dominated by violet and blue emissions was observed from all ZnO QD–SiO_xN_y nanocomposite films with dot diameters ranging from 2.77 to 6.65 nm. X-ray photoemission spectroscopy (XPS) revealed the formation of nitrogen-correlated bonding configurations in both the SiO_xN_y matrix and the dot/matrix interfaces. The nitrogen-correlated configuration at the interface produced a substantial polarization effect at dot surface. The suppression of green-yellow emission observed in photoluminescence spectra of all samples was ascribed to the hole-trapping process promoted by the enhancement of the surface polarization.

I. INTRODUCTION

Recently, semiconductor quantum dots (QDs) embedded in various dielectric materials have attracted considerable research interest. Apart from quantum confinement due to the nanometer dimension,[1] semiconductor QDs embedded in a dielectric material experience specific effects such as dielectric confinement[2–7] and surface polarization at the surface of QDs.[8–10] The influences of dielectric environment on optical properties of nanostructured semiconductors have been discussed.[11–13] Implanting nanostructured semiconductors into specific dielectrics produces composite materials with unique luminescence properties; their applications to optoelectronic devices and biosensors have been demonstrated. For instance, the CdSe-dielectric system may serve as an active medium in tunable lasers to achieve full-color emission.[14,15]

Similar to CdSe-dielectric systems, ZnO-dielectric systems with distinct luminescent properties have been developed.[16–19] One advantage of the ZnO-dielectric systems is that it does not suffer severe oxidation and degradation as in the CdSe-dielectric system. Moreover, the wide band gap (E_g = 3.25 to 3.5 eV) and large exciton binding energy (59 meV) of ZnO allow ZnO-dielectric systems to exhibit a high luminescence efficiency at room temperature. At present, the ZnO–SiO_2 composite prevails over other ZnO-dielectric systems because it can be prepared through several methods, such as sol-gel,[20,21] molecular capping,[22] impregnation method,[23] etc. In previous studies, we prepared the ZnO QDs–SiO_2 nanocomposite films with dot diameters ranging from 1.96 to 6.54 nm by a target-attached sputtering method.[24,25] Gaussian curve fitting of photoluminescence (PL) spectra showed that the integrated intensities of three emission bands from ZnO QDs–SiO_2 nanocomposite films vary with the surface-to-volume ratio (SV ratio) of QDs. An analysis of luminescent intensity in relation to defect energy levels indicated that the mechanisms of emission transitions are strongly affected by the presence of ZnO/SiO_2 interfaces. Consequently, we prepared ZnO QDs–SiO_xN_y nanocomposite films and investigated their luminescent properties and microstructures to explore the effects of dielectric matrix type on the photoemission mechanisms of ZnO QD. Our analysis of the photoelectron signals reveals the chemical bonding structures in these nanocomposite samples and derives specific bonding configurations correlating to nitrogen at the ZnO QDs–SiO_xN_y interface. The incorporation of nitrogen atoms at the dot/matrix interface and its influence on the luminescent properties of ZnO QDs–SiO_xN_y nanocomposite films are also discussed.

[a)]Address all correspondence to this author.
e-mail: tehsieh@mail.nctu.edu.tw
DOI: 10.1557/JMR.2008.0134

II. EXPERIMENTAL DETAILS

The ZnO–SiO_xN_y nanocomposite films containing ZnO QDs with diameters ranging from 2.77 to 6.65 nm were fabricated by target-attached sputtering. The samples were prepared by attaching ZnO (99.999%) pellets in adequate area proportions on a Si_3N_4 (99.5%, 51 mm) target during sputtering deposition under these conditions: radio frequency (rf) power, 50–200 W; flowing gas, Ar + 2.5% N_2; working pressure, 3–10 mTorr. Si wafers were adopted as substrates; neither substrate heating nor postannealing was performed. As the Si in Si_3N_4 can combine with O^- or O^{2-} from ZnO pellets or from residual CO_3^{2-} in the vacuum chamber to produce SiO_x during sputtering, the dielectric matrix of the nanocomposite films is thus metastable SiO_xN_y instead of pure Si_3N_4.

The microstructure of the samples was characterized with a transmission electron microscope (TEM; Philips TECNAI 20 FEG) (Eindhoven, The Netherlands). The chemical bonding was examined with x-ray photoemission spectroscopy (XPS) recorded with a Mg K_α source (American Physical Electronics ESCA PHI 1600) (Chanhassen, MN). The PL spectra were measured at room temperature using a He–Cd laser with emitting wavelength of 325 nm.

III. RESULTS AND DISCUSSION

A. Microstructure of ZnO–SiO_xN_y nanocomposites

Figure 1(a) shows the TEM micrographs of ZnO QDs–SiO_xN_y nanocomposite films containing ZnO QDs of various sizes. The density of ZnO QDs increases as the dot size increases from 2.77 to 6.65 nm. A typical selected-area electron diffraction (SAED) pattern of nanocomposite film presented in Fig. 1(b) indicates that the nanoscale ZnO QDs are crystalline[25] rather than amorphous clusters. TEM characterization also revealed that, though the ZnO QDs–SiO_xN_y and ZnO QDs–SiO_2 systems possess similar microstructures, the thermal stability of SiO_xN_y matrix seems inferior to that of SiO_2 matrix. During electron bombardment, the ZnO QDs–SiO_xN_y films were prone to break, and pores developed in TEM samples. This is attributed to the absorption of thermal energy by dangling bonds in the SiO_xN_y matrix which, in turn, results in the contraction of samples.

Figure 2 displays the histograms of ZnO dot size deduced from the TEM characterizations on the samples shown in Fig. 1(a). The sizes of over 80 ZnO dots were measured in each sample, and the distribution was fitted by a Gaussian function. It was found that the samples with small dot sizes and low dot densities contained well-separated ZnO QDs with narrow distributions of size. For samples with large dot sizes and high dot densities, neighboring ZnO dots tended to coalesce and become large crystalline clusters.

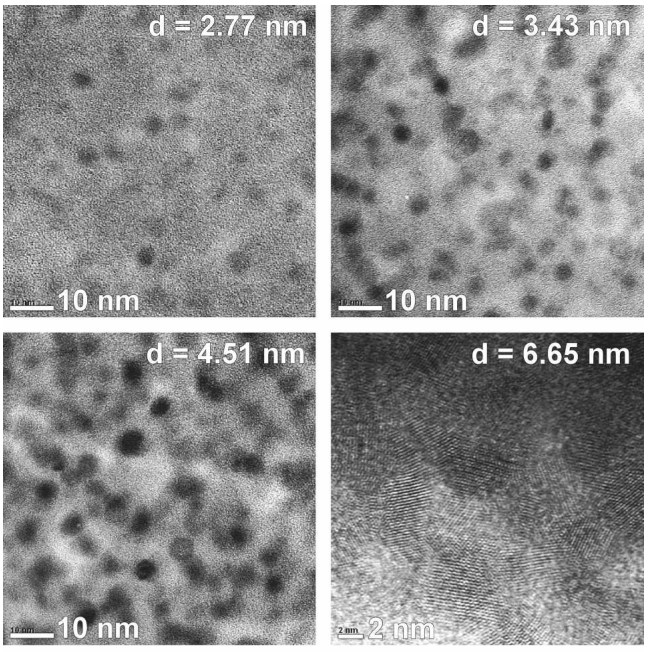

FIG. 1. (a) TEM images of ZnO QDs–SiO_xN_y nanocomposite films containing ZnO QDs with dot diameters ranging from 2.77 to 6.65 nm. (b) A typical SAED pattern of ZnO QDs–SiO_xN_y nanocomposite films containing.

B. PL spectra and Gaussian curve fittings

PL spectra of ZnO QDs–SiO_xN_y nanocomposite films are shown in Fig. 3(a). There is no significant variation of the shape of spectra for all samples, but the luminescence intensities vary with dot sizes. The green-yellow emissions in the ZnO QDs–SiO_xN_y system are less intense than those observed in the ZnO QDs–SiO_2 system,[24,25] even for those samples with severe coalescence of dots. The green-yellow emission is attributed to $V_O^{\cdot}/V_O^{\cdot\cdot}$ residing in the bulk region of QD, whereas the violet and blue emissions are related to surface states or V_{Zn} acceptors at the dot surface.[24,25] In contrast to ZnO QDs–SiO_2 films,[24,25] there is no extra or absent emission in the PL spectra of ZnO QDs–SiO_xN_y films, implying that the change of dielectric matrix type creates no new defect species in ZnO QD.

The optimized Gaussian curve fitting of PL spectra was performed under the constraint $w_{violet} \approx w_{blue}$

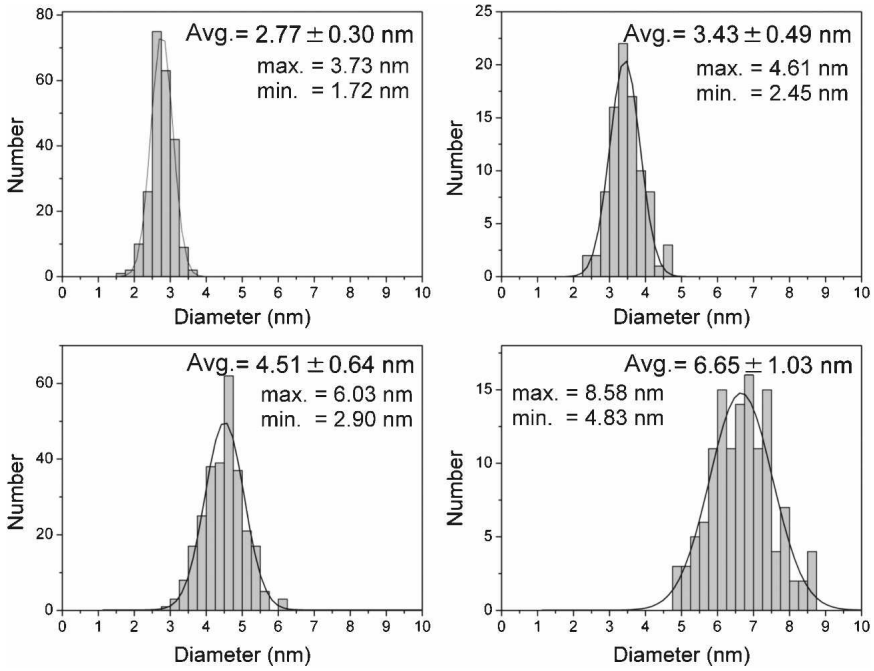

FIG. 2. Histograms of ZnO dot sizes deduced from the TEM characterizations on the samples shown in Fig. 1(a).

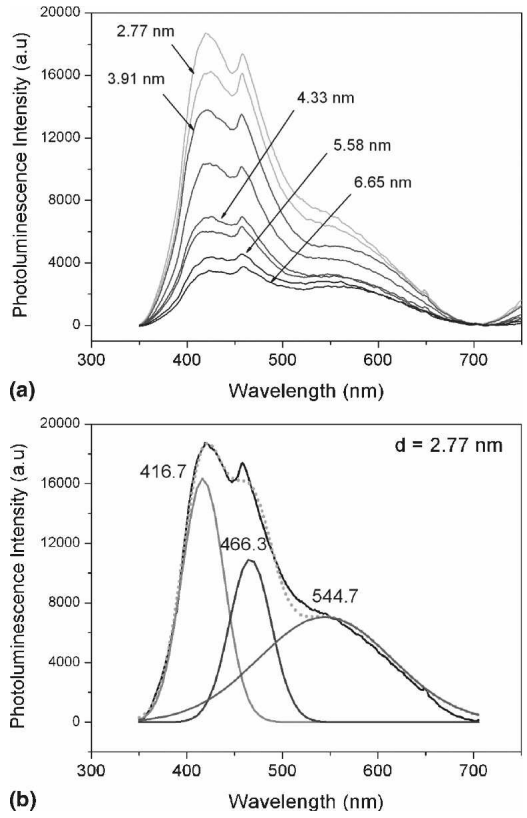

FIG. 3. (a) PL spectra of ZnO QDs–SiO_xN_y nanocomposite films with dot diameters ranging from 2.77 to 6.65 nm. (b) An example of Gaussian curve fitting of PL spectra consisting of violet, blue, and green-yellow emission bands.

(w = bandwidth of emission band). As illustrated in Fig. 3(b), the spectrum contains three emission bands, i.e., violet, blue, and green-yellow bands, with corresponding photon energies about 2.98, 2.66, and 2.28 eV, respectively. The peak position and bandwidth of each emission versus the dot diameter deduced from the curve fitting of PL spectra are presented in Figs. 4(a) and 4(b). These interband transitions of ZnO QDs–SiO_xN_y films exhibit no significant blue shift as the dot size decreases. We speculated that these defect levels or trap states might be affected or pinned by the surface/interface bonding configurations, especially for small dots, and result in a band shift behavior of the interband transition dissimilar to that of a near-band-edge transition.[25] The dependence of integrated intensity of the violet and blue emissions on the SV ratio are shown in Fig. 4(c). It can be seen that the integrated intensities of the green-yellow emission for ZnO QDs–SiO_xN_y films are smaller than that for the ZnO QDs–SiO_2 films.[24,25] Such a distinct variation can be seen by comparing the peak intensities of the two nanocomposite systems. For ZnO QDs–SiO_xN_y film with dot diameter of 2.77 nm, the peak intensity of the violet emission is about 2.3 times that of the green-yellow emission, while for ZnO QDs-SiO_2 film with a comparable dot size, the peak intensities of the two peaks are nearly the same.

C. XPS analysis of the bonding characteristics of nanocomposite samples

The chemical compositions of a ZnO QDs–SiO_xN_y nanocomposite films were identified with the aid of XPS

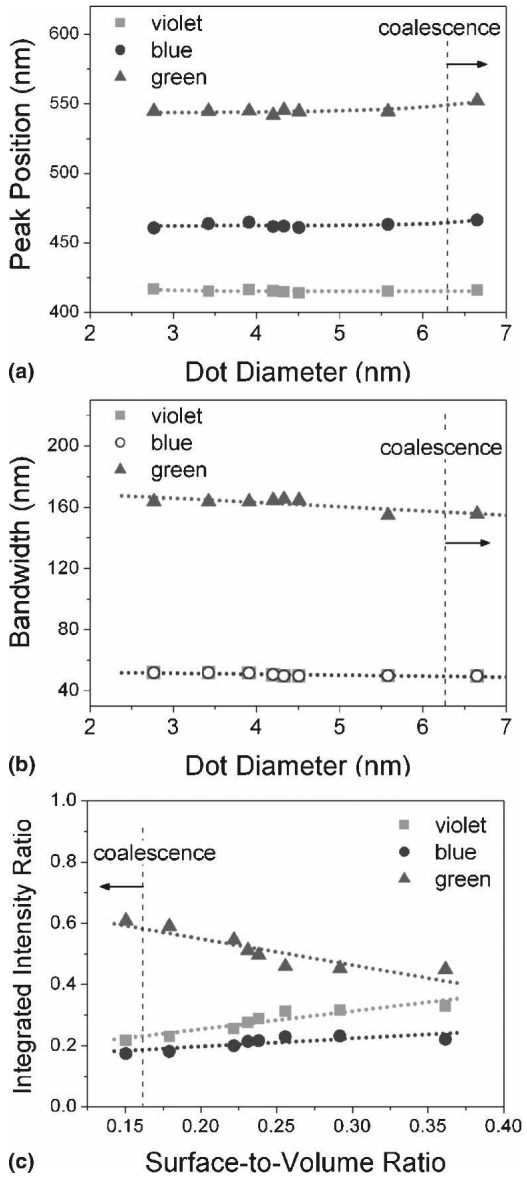

FIG. 4. Plots of (a) peak position and (b) bandwidth versus dot diameter and (c) integrated intensity ratio of emission band versus surface-to-volume ratio (SV ratio) deduced from the Gaussian curve fitting of PL spectra.

analysis. According to XPS data, the binding energy (E_b) of Zn $2p_{3/2}$ (1022.20 ± 0.10 eV) in ZnO QDs–SiO_xN_y (not shown) is identical to that observed in the ZnO QDs–SiO_2 system, implying a formation of the Zn^{2+} valence state in oxygen-deficient ZnO_{1-x}.[26] The photoemissions corresponding to Si, N, and O atomic levels are, however, rather complicated because of the presence of oxygen-containing ZnO and SiO_xN_y matrix in which the SiO_xN_y matrix might contain more than one chemical component, as described below.

An analysis of the O 1*s* atomic level in ZnO has been reported elsewhere.[24] Two oxygen species are present in ZnO[27]: the lattice oxygen $O_{lattice}$ (O1) denoted by O^{2-} in the crystalline network (530.1–530.4 eV), and O^- ions (O2) residing at sites at which the coordination number of oxygen ions is smaller than that at a regular site, e.g., subsurface (531.2–531.7 eV). Investigations of O 1*s* atomic level in SiO_xN_y matrix (O3) by characterizing the allotropes with various chemical stoichiometries have been reported previously.[28–33] Major differences between the photoemission signals of SiO_xN_y glass was ascribed to the varied bonding structures of basic units. In SiO_xN_y glass, the atomic configuration might contain oxygen-bridged (SiO_4)-structural units, tetrahedral (SiN_4)-units linked by a nitrogen atom, and their complexes.[29–33] Generally, a Si 2*p* atomic level in SiO_xN_y (Si1) has E_b lying in between the values for pure Si_3N_4 and for pure SiO_2 (Si2), i.e., 101.7–103.3 eV, whereas E_b of O 1*s* in SiO_xN_y (O3) shifts slightly to values less than that in SiO_x due to the competition of the electron affinity with the nitrogen atom. E_b of N 1*s* exhibits a strong dependence on chemical stoichiometry that corresponds to the combinations with varied amounts or types of atomic bonding. The N–Si_3/N–$(SiO_x)_3$ (N1) and Si_2–N–O (N2) exhibit distinct binding energies because of a severe chemical shift (1.7–2.0 eV) by the presence of the N–O bond.[29–33] Table I summarizes the E_b of Si *2p*, N 1*s*, and O 1*s* with the correlated atomic bonding in the ZnO QDs–SiO_xN_y system.

The XPS curves were analyzed (curve fitting program XPSPEAK 4.1) with a combination of Gaussian (80%) and Lorentzian (20%) distributions. Figures 5(a), 5(b), and 5(c) show the XPS features of Si 2*p*, N 1*s*, and O 1*s* atomic levels, respectively. The Si 2*p* spectra have two components: Si1 represents the (SiO_4)-units and Si2 originates from the SiO_xN_y-like component. Figure 5 indicates that there are fewer pure (SiN_4)-units (~101.7 eV) in samples because of the large population of O atoms. Hence the (SiO_4)-units decrease as the Si content decreases, implying that the matrix prefers the SiO_2–SiO_xN_y state at a high Si content (i.e., low proportion of ZnO) and switches to the SiO_xN_y state at a low Si content (i.e., high proportion of ZnO). The variation between the two nitrogen components (N1 and N2) as the Si content decreases can be readily seen in the fitted spectra [Fig. 5(b)] with an increasing tendency of the atomic combination from an N–Si bond to an N–O bond. A small

TABLE I. Summary of binding energies of Si 2*p*, N 1*s*, and O 1*s* atomic levels in ZnO[26,27] and SiO_xN_y materials.[28–33]

	Binding energy, E_b (eV)		
Materials	Si 2*p*	N 1*s*	O 1*s*
ZnO	…	…	530.0–530.4 (O1) 531.1–531.7 (O2)
Si_3N_4	101.7	397.4	…
SiO_xN_y	101.7–103.3 (Si1)	397.4–398.4 (N1) 399.0–401.0 (N2)	532.0–534.3 (O3)
SiO_2	103.3 (Si2)	…	532.5–534.3

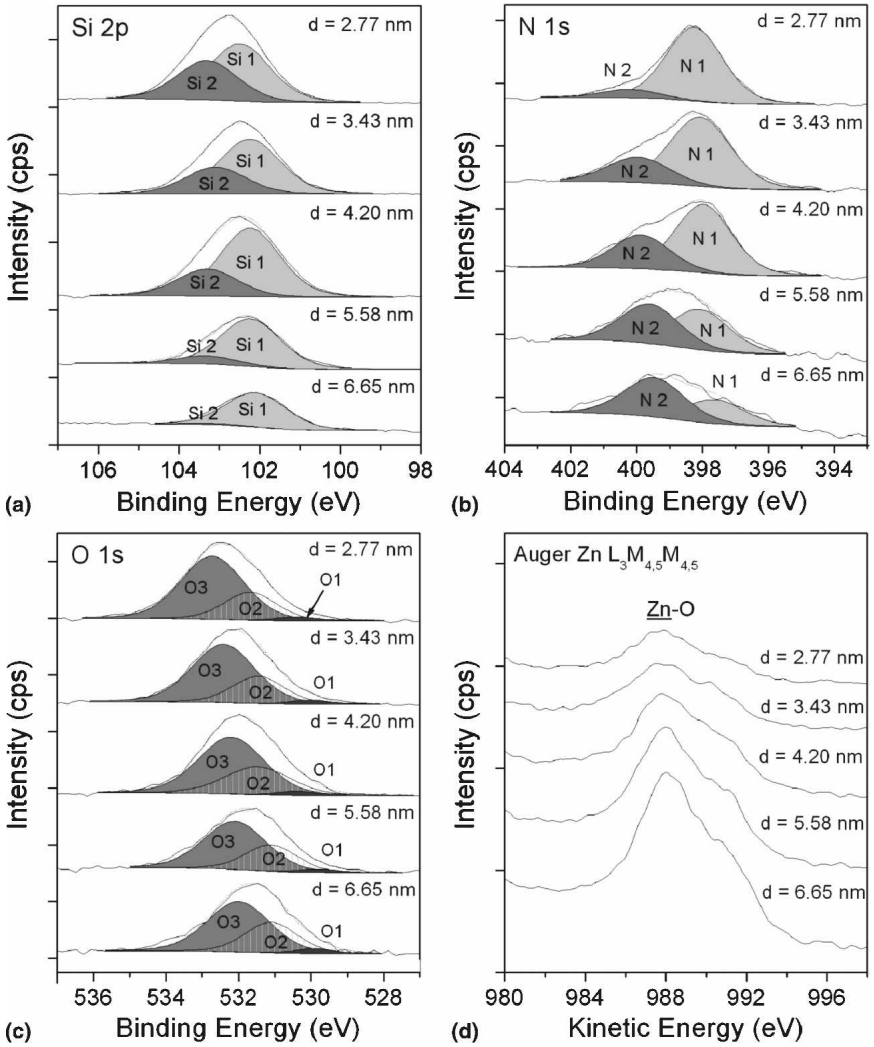

FIG. 5. Analytical results of XPS spectra for (a) Si 2*p*, (b) N 1*s*, and (c) O 1*s* atomic levels of ZnO QDs–SiO_xN_y nanocomposite films. (d) Auger Zn $L_3M_{4,5}M_{4,5}$ spectra of nanocomposite films.

reduction of the O3 component relative to the O2 component is revealed by Fig. 5(c), and the E_bs also slightly decrease as a result of the increasing N–O bonds. In consequence, oxygen atoms are allowed to form O–Si bonds in the samples with high Si content, whereas at low Si content, nitrogen atoms are prone to form N–O bonds with the loosely bound oxygen species in the samples.

The bonding state of ZnO was also characterized by analyzing the Auger Zn $L_3M_{4,5}M_{4,5}$ spectra as they are more sensitive to the variation of the chemical environment than the Zn 2*p* spectra. Figure 5(d) shows Auger Zn $L_3M_{4,5}M_{4,5}$ spectra of ZnO QDs–SiO_xN_y films. In all samples, the Auger peaks at about 988.1 eV clearly reveal the presence of Zn–O bonds in the oxide state. Moreover, the absence of Zn–N bonds[34,35] in the spectra indicates no nitrogen-doping in ZnO QD, even with the introduction of nitrogen gas flowing during sputtering. Thus the suppression of the green-yellow emission was not originated from the *p*-type doping of ZnO; i.e., no shallow acceptor N_O formed in ZnO QDs embedded in the SiO_xN_y matrix.[36,37]

D. N-correlated bonding configuration at the dot/matrix interface

Theoretical calculations showed that the N1 component possesses a binding energy shift (+0.19 to +0.66 eV) relative to interfacial N atoms in the $N–Si_3$ configuration due to the presence of N atoms in the SiO_2 matrix [i.e., the formation of $N–[Si(O–)_3]_3$ configuration].[38,39] According to this finding, two bonding components, N1 and N2, in the ZnO QDs–SiO_xN_y system were obtained by fitting the N 1*s* XPS spectra. Figure 5(b) reveals that, as the dot size and density increase (i.e., when the Si content decreases), the N1 component decreases, whereas the N2 component increases. In contrast, the trend of the increasing N2 component indicates a distinct chemical bonding configuration in the nanocomposite samples. In addition

to an influence of the processing temperature,[32] the formation of the N2 component is specifically related to the interfacial region.[30,32,33] Kobayashi et al.[32] reported that the processing temperature affects both the activities of ionic bonding and the stoichiometry of the SiO_xN_y matrix, which, in turn, alters the proportion of the N2 component. During our sputtering deposition, there was no significant substrate temperature variation; the increase of the N2 component with increasing dot size and density was thus not induced by thermal effects. The incorporation of nitrogen atoms at the surface/interface was commonly observed in the nitridation of SiO_2 because of the smaller activation energy at the surface/interface region.[30,32,33] We thus speculated that the N2 component resides at the dot/matrix interfaces rather than in the matrix.

An incorporation of nitrogen atoms at the dot/matrix interface is also explicable through the large population of dangling O-bonds at the dot/matrix interface. Such dangling O-bonds are commonly observed at the SiO_2/Si interface that provides adsorption sites for certain species to be weakly bound. In the ZnO QDs–SiO_xN_y system, the O^- ions at the dot surface serve as dangling O-bonds, which attract nitrogen atoms to form N–O bonds or the N2 configuration. The formation of such a nitrogen-correlated configuration is also promoted by the active N^+/N_2^+-plasma[31,32] generated by the introduction of nitrogen gas during sputtering as the N^+/N_2^+ species are readily attracted to O^- ions at the ZnO QD surface and induce the Si_2–N–O bonding.

E. Effects of surface polarization on photoemission property

Considering the analytical results described above, we propose a surface bonding configuration model for the ZnO QDs–SiO_xN_y system, as illustrated in Fig. 6(a). In Fig. 6(a), the O^- ion residing at the dot surface[27] might interact with the N2 component of the SiO_xN_y matrix to form an O(δ−)–N(δ+) bond. Figure 6(b) presents the surface bonding configuration model of the ZnO QDs–SiO_2 system for the purpose of comparison. In such a system, the O^- ions at the dot surface incorporate with the (SiO_4)-units as an O–Si bond. The asymmetry of these bonding structures and the polarization direction normal to the QD surface depicted in Fig. 6 enable us to estimate the effective polarization in above two models. In Fig. 6(a), both O(δ−)–N(δ+) and N–Si bonds separately contribute a dipole moment in the direction toward the dot surface and thus amplify the surface polarization. In contrast, Fig. 6(b) shows that the dipole moments induced by O–Si and Si–O bonds lie in opposite directions with comparable magnitudes. They tend to cancel each other and leave a weak surface polarization. The N2-type configuration, O–N–Si_2, at the dot/matrix interface of the ZnO QDs–SiO_xN_y system consequently provides a greater surface polarization in comparison with the O–Si–O_3 configuration of the ZnO QDs–SiO_2 system.

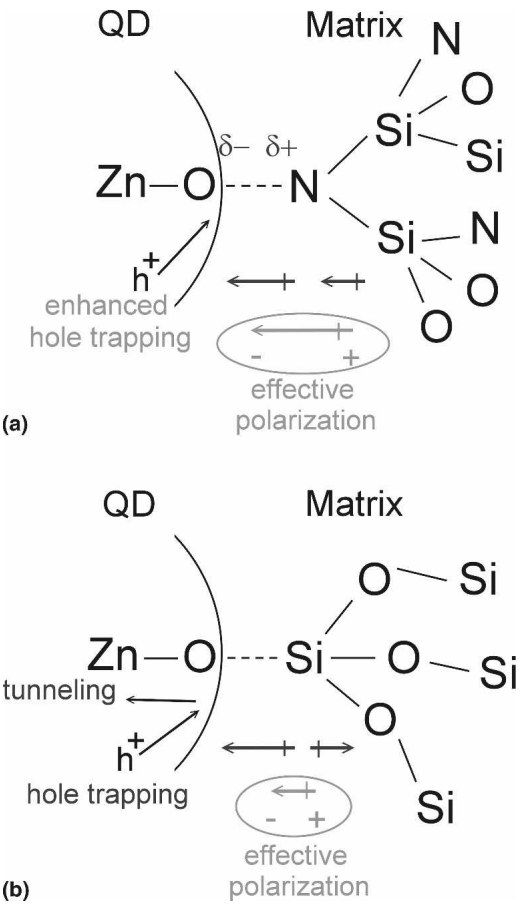

FIG. 6. Surface bonding configuration models at the ZnO QD/dielectric interface for (a) ZnO QDs–SiO_xN_y and (b) ZnO QDs–SiO_2 systems.

The atomic configuration at the dot surface with the complicated dielectric matrix, resulting in an amplified surface polarization, is known to affect the carrier transport in a specific manner.[40] As already reported, the green-yellow emission is ascribed to a radiative recombination of an electron from the conduction band with a deep trap level $V_O^{\cdot\cdot}$. The recombination center $V_O^{\cdot\cdot}$ is formed as a result of a $V_O^{\cdot} \rightarrow V_O^{\cdot\cdot}$ transition promoted by the hole trapping/tunneling of O_i^n/O_i' at the dot surface.[41] We speculated that the reinforced surface polarization promotes hole trapping at the dot surface and inhibits the tunneling, i.e., the $V_O^{\cdot} \rightarrow V_O^{\cdot\cdot}$ transition. Such a surface polarization retards the transition rate of an electron from the conduction band to the deep trap level, thereby suppressing the green-yellow emission of ZnO QD.

IV. CONCLUSIONS

ZnO QDs–SiO_xN_y nanocomposite films were prepared via target-attached rf sputtering without substrate heating

and post annealing. PL measurement revealed the same increasing tendency of violet and blue emissions with an increased SV ratio, as observed in the ZnO QDs–SiO_2 system. The XPS analyses illustrated both the chemical bonding complexity in the SiO_xN_y matrix and the specific bonding configurations at the dot/matrix interface generate a strong surface polarization on the ZnO QDs. Such a surface polarization reinforces hole trapping and thus inhibits the green-yellow band transition in the ZnO QDs–SiO_xN_y nanocomposite samples. This work not only demonstrates the versatile luminescent properties of ZnO QDs-dielectric nanocomposite systems but also illustrates the promising applicability of semiconductor QDs in the fields of optoelectronic and solid-state lighting.

ACKNOWLEDGMENT

This work was supported by National Science Council (NSC), Taiwan, Republic of China under the Contract Nos. NSC95-2221-E009-130 and NSC95-2112-M213-005.

REFERENCES

1. A.P. Alivisatos: Semiconductor clusters, nanocrystals and quantum dots. *Science* **271,** 933 (1996).
2. L.E. Brus: A simple model for the ionization potential, electron affinity, and aqueous redox potentials of small semiconductor crystallites. *J. Chem. Phys.* **79,** 5566 (1983).
3. D. Babić, R. Tsu, and R.F. Greene: Ground-state energies of one- and two-electron silicon dots in an amorphous silicon dioxide matrix. *Phys. Rev. B* **45,** 14150 (1992).
4. M. Iwamatsu, M. Fujiwara, N. Happo, and K. Horii: Effects of dielectric discontinuity on the ground-state energy of charged Si dots covered with a SiO_2 layer. *J. Phys.: Condens. Matter* **9,** 9881 (1997).
5. A. Franceschetti and A. Zunger: Pseudopotential calculations of electron and hole addition spectra of InAs, InP, and Si quantum dots. *Phys. Rev. B* **62,** 2614 (2000).
6. A. Franceschetti and A. Zunger: Addition energies and quasiparticle gap of CdSe nanocrystals. *Appl. Phys. Lett.* **76,** 1731 (2000).
7. A. Orlandi, M. Rontani, G. Goldon, F. Manghi, and E. Molinari: Single-electron charging in quantum dots with large dielectric mismatch. *Phys. Rev. B* **63,** 045310 (2001).
8. L. Bányai, P. Gilliot, Y.Z. Hu, and S.W. Koch: Surface-polarization instabilities of electron-hole pairs in semiconductor quantum dots. *Phys. Rev. B* **45,** 14136 (1992).
9. A. Orlandi, G. Goldoni, F. Manghi, and E. Molinari: The effect of dielectric polarization-induced surface states on many-body configurations in a quantum dot. *Semicond. Sci. Technol.* **17,** 1302 (2002).
10. N.V. Tkach and R.B. Fartushinski: Influence of phonons on the electronic energy spectrum of small semiconductor quantum dots in a dielectric matrix. *Phys. Solid State* **45,** 1347 (2003).
11. A. Bsiesy, F. Muller, M. Ligeon, F. Gaspard, R. Hérino, R. Romestain, and J.C. Vial: Relation between porous silicon photoluminescence and its voltage-tunable electroluminescence. *Appl. Phys. Lett.* **65,** 3371 (1994).
12. J. Linnros, N. Lalic, P. Kánpek, K. Luterová, J. Kočka, A. Fejfar, and I. Pelant: Instabilities in electroluminescent porous silicon diodes. *Appl. Phys. Lett.* **69,** 833 (1996).
13. R.T. Collins, P.M. Fauchet, and M.A. Tischler: Porous silicon: From luminescence to LED. *Phys. Today* **50,** 24 (1997).
14. J. Lee, V.C. Sundar, J.R. Heine, M.G. Bawendi, and K.F. Jensen: Full color emission from II-VI semiconductor quantum dot–polymer composites. *Adv. Mater.* **12,** 1102 (2000).
15. S.T. Selvan, C. Bullen, M. Ashokkunar, and P. Mulvaney: Synthesis of tunable, highly luminescent QD-glasses through sol-gel processing. *Adv. Mater.* **13,** 985 (2001).
16. L. Guo, S. Yang, C. Yang, P. Yu, J. Wang, W. Ge, and G. Wong: Synthesis and characterization of poly(vinylpyrrolidone)-modified zinc oxide nanoparticles. *Chem. Mater.* **12,** 2268 (2000).
17. L. Guo, S. Yang, C. Yang, P. Yu, J. Wang, W. Ge, and K.L. Wong: Highly monodisperse polymer-capped ZnO nanoparticles: preparation and optical properties. *Appl. Phys. Lett.* **76,** 2901 (2000).
18. M. Abdullah, T. Morimoto, and K. Okuyama: Generating blue and red luminescence form ZnO/Poly(ethyleneglycol) nanocomposites prepared using in-situ method. *Adv. Funct. Mater.* **13,** 800 (2003).
19. S. Das, S. Chakrabarti, and S. Chaudhuri: Optical transmission and photoluminescence studies of ZnO–MgO nanocomposite thin films. *J. Phys. D: Appl. Phys.* **38,** 4021 (2005).
20. S. Charkrabarti, D. Das, D. Ganguli, and S. Chaudhuri: Tailoring of room temperature excitonic luminescence in sol-gel zinc oxide-silica nanocomposite films. *Thin Solid Films* **441,** 228 (2004).
21. H. He, Y. Wang, and Y. Zou: Photoluminescence property of ZnO–SiO_2 composites synthesized by a sol-gel method. *J. Phys. D: Appl. Phys.* **36,** 2972 (2003).
22. J. Bang, H. Yang, and H. Holloway: Enhanced luminescence of SiO_2:Eu^{3+} by energy transfer form ZnO nanoparticles. *J. Chem. Phys.* **123,** 084709 (2005).
23. L. Xiong, J. Shi, J. Gu, L. Li, W. Shen, and Z. Hua: Co-templating synthesis of highly dispersed 1D ZnO nanostructures in amorphous SiO_2 under hydrothermal conditions. *Solid State Sci.* **6,** 1341 (2004).
24. Y-Y. Peng, T-E. Hsieh, and C-H. Hsu: White-light emitting ZnO–SiO_2 nanocomposite thin films prepared by target-attached sputtering methods. *Nanotechnology* **17,** 174 (2006).
25. Y-Y. Peng, T-E. Hsieh, and C-H. Hsu: Optical characteristics and microstructure of ZnO quantum dots–SiO_2 nanocomposite films prepared by sputtering methods. *Appl. Phys. Lett.* **89,** 211909 (2006).
26. S. Major, S. Kumar, M. Bhatnagar, and K.L. Chopra: Effect of hydrogen plasma treatment on transparent conducting oxides. *Appl. Phys. Lett.* **49,** 394 (1986).
27. J.C. Dupin, D. Gonbeau, P. Vinatier, and A. Levasseur: Systematic XPS studies of metal oxides, hydroxides and peroxides. *Phys. Chem. Chem. Phys.* **2,** 1319 (2000).
28. R. Franke, C. Girgenrath, S. Kohn, and M. Jansen: An *x*-ray photoelectron spectroscopic study of novel SiON glasses. *Fresenius J. Anal. Chem.* **361,** 587 (1998).
29. J. Ushio, T. Maruizumi, and K.K. Abdelghafar: Interface structures generated by negative-bias temperature instability in Si/SiO_2 and Si/SiO_xN_y interfaces. *Appl. Phys. Lett.* **81,** 1818 (2002).
30. S. Shinagawa, H. Nohira, T. Ikuta, M. Hori, M. Kase, and T. Hattori: Angle-resolved XPS study on chemical bonds in ultrathin silicon oxynitride films. *Microelectron. Eng.* **80,** 98 (2005).
31. J.W. Kim, H.W. Yeom, Y.D. Chung, K. Jeong, and C.N. Whang: Chemical configuration of nitrogen in ultrathin Si oxynitride on Si(100). *Phys. Rev. B* **66,** 035312 (2002).
32. H. Kobayashi, T. Mixokuro, Y. Nakato, K. Yoneda, and Y. Todokoro: Nitridation of silicon-oxide layers by nitrogen

plasma generated by low-energy electron impact. *Appl. Phys. Lett.* **71,** 1978 (1997).

33. J.P. Chang, M.L. Green, V.M. Donnelly, R.L. Opila, J. Eng, Jr., J. Sapjeta, H.C. Lu, T. Gustafsson, and E. Garfunkel: Profiling nitrogen in ultrathin silicon oxynitrides with angle-resolved x-ray photoelectron spectroscopy. *J. Appl. Phys.* **87,** 4449 (2000).
34. M. Futsuhara, K. Yoshioka, and O. Takai: Optical properties of zinc oxynitride thin films. *Thin Solid Films* **317,** 322 (1998).
35. M. Futsuhara, K. Yoshioka, and O. Takai: Structural, electrical and optical properties of zinc nitride thin films prepared by reactive rf magnetron sputtering. *Thin Solid Films* **322,** 274 (1998).
36. K. Thonke, T. Gruber, N. Trofilov, R. Schönfelder, A. Waag, and R. Sauer: Donor-acceptor pair transitions in ZnO substrate material. *Physica B (Amsterdam)* **308,** 945 (2001).
37. Ü. Özgür, Y.I. Alivov, C. Liu, A. Teke, M.A. REshchikov, S. Doğan, V. Avrutin, S–J. Cho, and H. Morkoç: A comprehensive review of ZnO materials and devices. *J. Appl. Phys.* **98,** 041301 (2005).
38. G.F. Cerofolini, A.P. Caricato, L. Meda, N. Re, and A. Sgamellotti: Quantum-mechanical study of nitrogen bonding configurations at the nitrided Si–SiO_2 interface via model molecules. *Phys. Rev. B* **61,** 14157 (2000).
39. G-M. Rignanese, A. Pasquarello, J-C. Charlier, X. Gonze, and R. Car: Nitrogen incorporation at Si(001)–SiO_2 interfaces: Relation between N 1*s* core-level shifts and microscopic structure. *Phys. Rev. Lett.* **79,** 5174 (1997).
40. L. Bányai, P. Gilliot, Y.Z. Hu, and S.W. Koch: Surface-polarization instabilities of electron-hole pairs in semiconductor quantum dots. *Phys. Rev. B* **45,** 14136 (1992).
41. A.V. Dijken, E.A. Meulenkamp, D. Van Maekelbergh, and A. Meijerink: The luminescence of nanocrystalline ZnO particles: The mechanism of the ultraviolet and visible emission. *J. Lumin.* **87,** 454 (2000).